Materials Research Bulletin 64 (2015) 347–354

Contents lists available at ScienceDirect

Materials Research Bulletin

journal homepage: www.elsevier.com/locate/matresbu

Hyperfine and magnetic properties of a $Y_xLa_{1-x}FeO_3$ series ($0 \leq x \leq 1$)

A.A. Cristóbal [a], P.M. Botta [a], P.G. Bercoff [b,*], C.P. Ramos [c]

[a] Instituto de Investigaciones en Ciencia y Tecnología de Materiales (INTEMA), CONICET-UNMdP, Av. J.B. Justo 4302, B7608FDQ Mar del Plata, Argentina
[b] Facultad de Matemática, Astronomía y Física (FaMAF), Universidad Nacional de Córdoba. IFEG (CONICET), Medina Allende s/n, Ciudad Universitaria, 5000 Córdoba, Argentina
[c] CONICET and Centro Atómico Constituyentes (CAC), CNEA, Av. Gral. Paz 1499, 1650 San Martín, Argentina

ARTICLE INFO

Article history:
Received 12 June 2014
Received in revised form 23 December 2014
Accepted 4 January 2015
Available online 12 January 2015

Keywords:
A. Ceramics
B. Powder metallurgy
C. Magnetometer
C. Mössbauer spectroscopy
D. Magnetic properties

ABSTRACT

A series of orthoferrites $Y_xLa_{1-x}FeO_3$ in the entire range of composition was synthesized at room temperature by mechanochemical activation of oxide mixtures. Phase composition, structure and microstructure of the obtained powder materials were characterized by X-ray diffraction and field-emission scanning electron microscopy. Hyperfine interactions and magnetic properties were determined by Mössbauer spectroscopy, SQUID and vibrating sample magnetometry. Two magnetic contributions could be identified in the series of materials: a paramagnetic state, associated with a fraction of the smallest particles and a ferromagnetic state, attributed to the larger particles. The results showed that the relative proportion of both contributions is very dependent on *x*, the Y content of samples. From *M* vs *T* measurements, it was possible to estimate the blocking temperature distribution for the end members of the series. Annealing of samples produced the elimination of the superparamagnetic behavior and the formation of $Y_3Fe_5O_{12}$ impurities.

1. Introduction

Orthoferrites with general formula $AFeO_3$ are a prominent family of inorganic compounds, because of the plethora of properties and applications that they often exhibit. In most cases, they crystallize in a perovskite-type structure, with corner-sharing FeO_6 octahedra and A cations occupying the center of a cube (generally with an orthorhombic or rhombohedral distortion) [1]. From a technological point of view, materials based on orthoferrites are interesting because they can be used in a wide range of applications: sensors, catalysts, solid oxide fuel cells, etc [2–4]. Their functional properties (electrical conductivity, magnetization, catalytic activity) are very dependent on the structure, which can be significantly modified through the incorporation of cations with different sizes and charges [5–7]. Frequently, the size of cation A determines the structure adopted by orthoferrites, being ideal perovskite structures (cubic) or distorted ones (tetragonal, orthorhombic, rhombohedral). The distortion is produced by the cooperative tilting of FeO_6 octahedra around their own axes [8]. In order to estimate the distortion degree, the tolerance factor of Goldschmidt (*t*) [9] can be calculated using adequate values of ionic radii (frequently radii provided by Shannon [10]). When $t = 1$, orthoferrites crystallize in a cubic structure, and when *t* decreases (not lower than 0.75) the lattice has an orthorhombic or rhombohedral symmetry.

$LaFeO_3$ and $YFeO_3$ are two perovskite-type ferrites, whose stable structures at room temperature have an orthorhombic crystal symmetry. The first one has in fact a quasi-tetragonal structure (lattice parameters *a* and *b* are almost identical) whereas the second one presents a lower symmetry, because of the less similarity between *a* and *b*. The magnetic structure of these compounds can be described as a two-sublattice system formed by FeO_6 octahedra strongly antiferromagnetically coupled and slightly canted, producing a net magnetic moment perpendicular to the antiferromagnetic axis. The canting angle is very small (milliradians) and depends on the A-cation size [11,12]. These features and the extraordinary domain-wall motion of these compounds make them suitable for magneto-optical devices, such as switches and sensors [13–15].

A wide and diverse variety of preparative routes has been used to produce $LaFeO_3$ and $YFeO_3$. Among them, conventional solid-state method, combustion synthesis, sol–gel, hydrothermal synthesis and co-precipitation technique have been mostly used [16–19]. Generally, micro or nanoparticles of $LaFeO_3$ can be easily obtained free of impurities. By contrast, preparation of $YFeO_3$ is often problematic, because the formation of the garnet $Y_3Fe_5O_{12}$ (YIG) competes in the reaction [20,21]. Other methods have demonstrated to be more efficient than solid-state reactions to

* Corresponding author. Tel.: +54 351 4334051x103; fax: +54 351 4334054.
E-mail address: bercoff@famaf.unc.edu.ar (P.G. Bercoff).

http://dx.doi.org/10.1016/j.materresbull.2015.01.014
0025-5408/

avoid or minimize this limitation [22–24]. Anyhow, Cristóbal et al. have reported a mechanically assisted solid-state route for producing both compounds, pure and nanocrystalline [25,26]. High-energy ball-milling of oxide precursors is a convenient way to favor the kinetics of solid-state reactions, commonly retarded by very slow ionic diffusion rates. Some of the operative advantages of this synthesis method are the possibility of obtaining relatively large amounts of powders, the occurrence of solid-state reactions at room temperature and the absence of organic solvents throughout the process [27–29]. On the other hand, the incorporation of large amounts of structural defects during the milling produces significant changes in the properties which are dependent on structural ordering, such as the magnetic ones [30–32]. In previous reports, we have shown the link between magnetic behavior and the alteration of crystal ordering provoked by the mechanochemical action in the synthesis of $LaFeO_3$, pure and modified with Y [26]. However, the extreme complexity of the system requires a deeper insight into the magnetic interactions, in order to properly understand the observed responses. Here we present a detailed investigation of hyperfine and magnetic properties of the series $Y_xLa_{1-x}FeO_3$ ($0 \le x \le 1$), synthesized by high-energy ball milling.

2. Experimental

Powder mixtures of Fe_3O_4 (a magnetite concentrate ore, 97.5%), La_2O_3 and Y_2O_3 (commercial reagents, 99.9%) with different molar ratio were prepared and mechanochemically activated in a Fritsch Pulverissette 7 planetary ball-mill using balls and vials made of Cr-hardened steel. A ball-to-powder mass ratio of 20 and a rotation speed of 1500 rpm were used. Oxygen supply was assured by periodically opening the vials, at the time that small portions of powder were withdrawn in order to follow the evolution of the activation process. Five compositions with yttrium contents (x in the formula $Y_xLa_{1-x}FeO_3$) ranging between 0 and 1 were ball-milled for 3 h. The activated powders were then thermally treated at 1000 °C for 30 min in air atmosphere. The series of as-milled samples was named YLM-x while the calcined samples were labeled YLM-x-1000, being x the Y content.

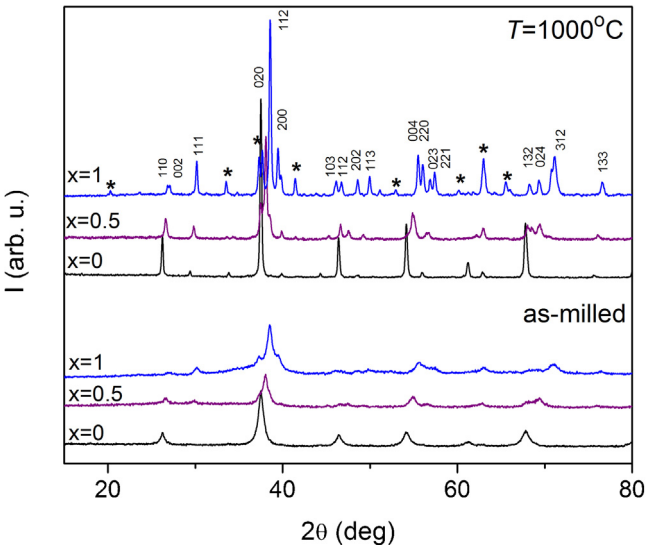

Fig. 1. XRD patterns for samples YML-x and YML-x-1000 (x = 0, 0.5 and 1) as-milled and heated at 1000 °C. Indexed peaks belong to $Y_xLa_{1-x}FeO_3$; peaks marked with * belong to YIG phase. (For interpretation of the references to colour in this figure legend, the reader is referred to the web version of this article.)

2.1. Characterization

The structure of crystalline phases was analyzed by X-ray diffraction (XRD) using a Philips PW 1830/40 diffractometer at 40 kV and 30 mA, with CoKα radiation (λ = 0.17890 nm) and Fe filter.

Magnetization (M) at room temperature as a function of applied field (H) was measured using a Lakeshore 7300 vibrating sample magnetometer. Magnetic loops between +15 and −15 kOe were registered. M vs T measurements were performed in a SQUID magnetometer (Quantum Design) under a zero-field cooling (ZFC)/field cooling (FC) regime.

Sample microstructures were studied by field emission gun scanning electron microscopy (FEG-SEM), using a Zeiss Supra40 electron microscope.

Mössbauer spectra were taken at room temperature (RT) and 20 K in a conventional constant acceleration spectrometer in transmission geometry with a ^{57}Co/Rh source. The absorber thickness was chosen to be the optimum according to the Long et al. criterion [33]. Least-squares fitting of the spectra was performed by using the Normos program [34]. Isomer shift (IS) values are given relative to that of α-Fe at room temperature.

3. Results and discussion

Fig. 1 shows the XRD patterns of the series of activated and calcined samples for x = 0, 0.5 and 1. The completion of the reaction is confirmed by the absence of reactants' peaks and the formation of the corresponding orthoferrite.

As x increases, additional peaks corresponding to $Y_xLa_{1-x}FeO_3$ appear as a consequence of the loss of crystalline symmetry. Also, a shifting to towards higher 2θ values with Y content is observed because of the smaller size of Y^{3+} cation in comparison with La^{3+} cation. [26]. The peaks' profile for the as-milled samples denotes a very small crystallite size, which grows after heating at 1000 °C. An estimation of crystallite size using the Scherrer equation gives 10 nm for the unheated samples and 50 nm for heated powders, approximately. The XRD pattern of sample YML-1–1000 shows small peaks (indicated with * in Fig. 1) corresponding to a secondary phase (YIG), a very common impurity in the synthesis of $YFeO_3$ [20,21].

Room temperature (RT) Mössbauer spectra for the as milled samples – in the whole composition range – were fitted to a doublet and to a hyperfine field distribution, reflecting a particle size distribution. Fig. 2 (left column) shows a comparison between the different spectra. An evident evolution is observed as Y content increases; the doublet grows monotonically in a linear way. Table 1 exhibits the hyperfine parameters obtained by the fitting procedure with their relative contributed areas, which are proportional to the concentration of the corresponding Fe species.

The hyperfine field distribution parameters are typical for Fe^{3+} in octahedral coordination, in accordance to the orthoferrite phase structure and as Y content increases its medium value, B_{hf}, diminishes (Fig. 2 and Table 1). This may be the consequence of a change in the super-transferred hyperfine field, arising from distortions in the Fe–O–Fe bond lengths and angles. These distortions are more likely in the smaller particles because surface effects are intensified.

The maxima of the magnetic hyperfine field distribution for samples YLM-0 (∼51 T) and YLM-1 (∼48 T) respectively are smaller than those of the bulk values reported in literature [35,36], suggesting small particle sizes.

In order to clarify the presence of the doublet, Mössbauer spectra were also taken at 20 K. As an example, Fig. 3 shows the spectra for sample YLM-1 at RT (a) and 20 K (b). At RT, part of the spectrum is magnetically split and as temperature is reduced to

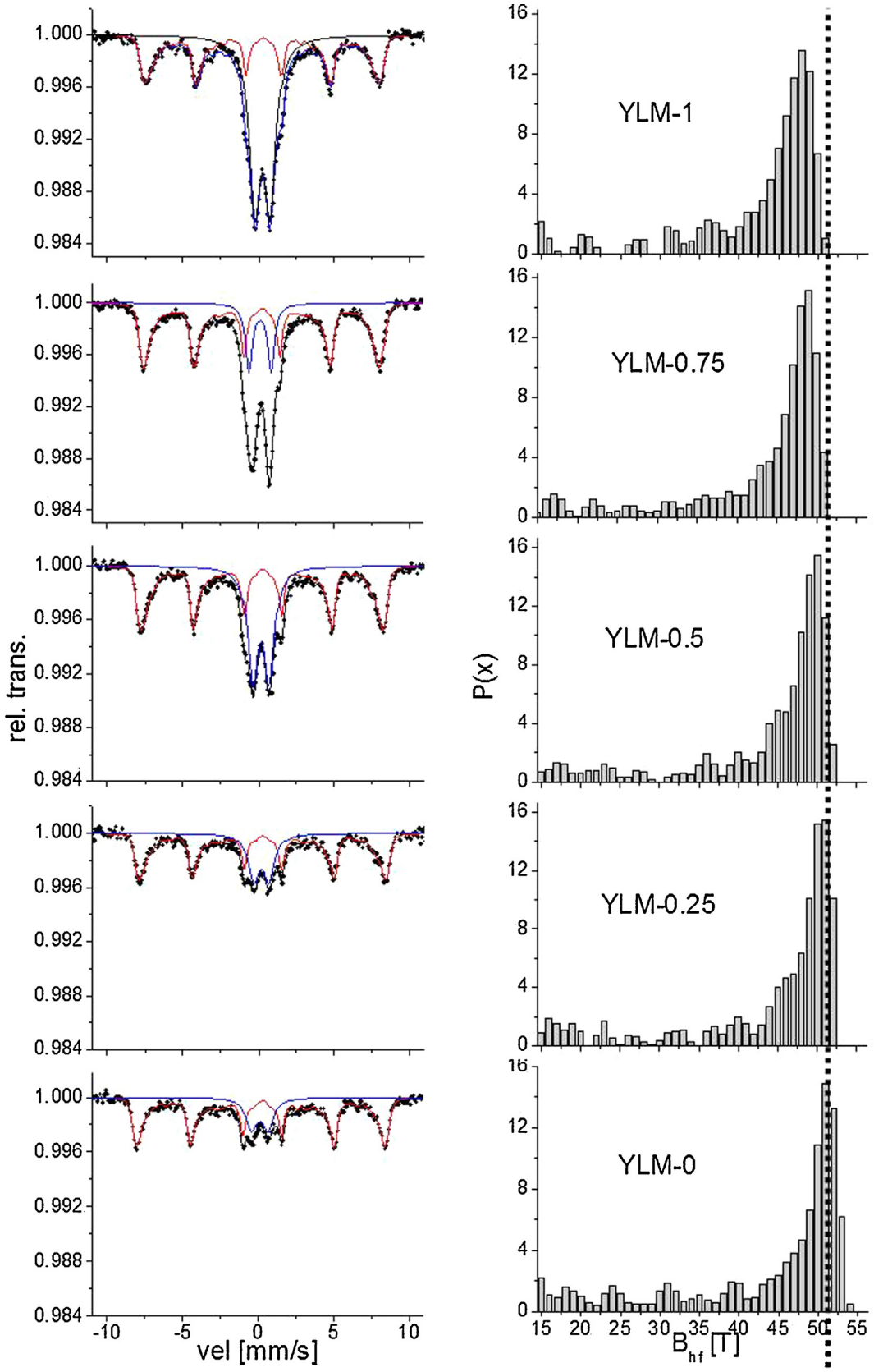

Fig. 2. Mössbauer spectra (left column) and their corresponding hyperfine field distributions (right column) for the whole as milled series. (For interpretation of the references to colour in this figure legend, the reader is referred to the web version of this article.)

Table 1
Mössbauer hyperfine parameters and relative abundance (%) of HF (hyperfine field) distributions and SPM (superparamagnetic) doublets. IS (isomer shift), QS (quadrupole splitting), 2ε (quadrupole shift), B_{hf} (median hyperfine magnetic field).

Sample	Contribution	IS (mm/s)	QS (mm/s)	2ε (mm/s)	B_{hf} (T)	(%)
YLM-0	HF distribution	0.36		−0.10	48.84	80
	SPM doublet	0.23	1.06			20
YLM-0.25	HF distribution	0.38		−0.04	48.58	70
	SPM doublet	0.30	1.03			30
YLM-0.50	HF distribution	0.37		−0.07	47.85	60
	SPM doublet	0.28	1.09			40
YLM-0.75	HF distribution	0.37		−0.04	46.96	50
	SPM doublet	0.29	1.13			50
YLM-1	HF distribution	0.39		−0.08	45.97	40
	SPM doublet	0.38	1.03			60

20 K this portion of the spectral area increases at the expense of the doublet component. The coexistence of magnetic and paramagnetic components in that temperature interval points out to a superparamagnetic behavior, typical for small magnetic particles which display a thermally fluctuating total moment. The whole series of samples reveals such a tendency.

From X-ray diffraction patterns it is clear that after three hours of mechanical treatment the signals corresponding to the reactants have disappeared and only peaks ascribed to orthoferrite can be observed (see Fig. 1). Then considering both, XRD and Mössbauer results, we can confirm that all the samples are single phase, excluding the presence of secondary phases in the reaction products.

In addition, the size and morphological characteristics of the prepared powders were examined by FEG–SEM (Fig. 4).

Micrographs revealed assemblies of roughly spherical and sub-micron agglomerates which, in turn, are composed of particles with mean diameter of 50 nm. These agglomerates seem to enlarge with Y content in the samples, reaching a diameter of approximately 500 nm.

Fig. 5 displays the hysteresis loops of the studied samples at RT. None of them saturate at the maximum applied field (1.5 T), probably due to the appreciable contribution of superparamagnetic particles. As Y content decreases, the loops get closer to saturation at 1.5 T, suggesting there are less superparamagnetic particles for smaller Y content. This has been confirmed by Mössbauer results (see Table 1). Coercivity H_c, remanence M and saturation magnetization M_s are shown in Table 2. This last value was calculated by extrapolating M vs $1/H$ to zero.

The obtained H_c value for sample YLM-1 (Table 2) is much lower than that of the corresponding nanocrystalline $YFeO_3$ (around 20 kOe) reported in the literature [23,37], although it is similar to

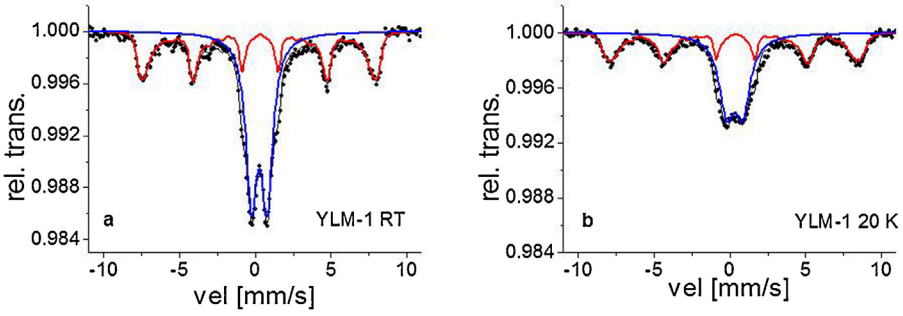

Fig. 3. Mössbauer spectra at RT (a) and 20 K (b) for sample YLM-1. (For interpretation of the references to colour in this figure legend, the reader is referred to the web version of this article.)

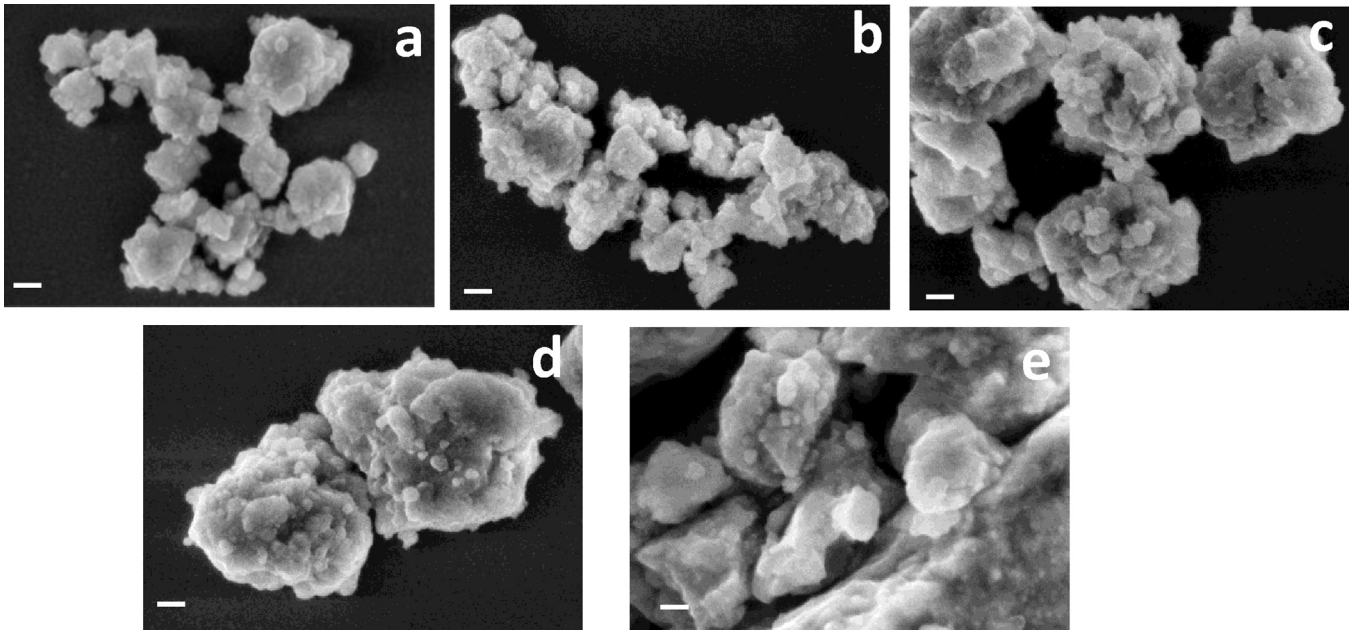

Fig. 4. FEG-SEM images obtained from samples with $x = 0$ (a), $x = 0.25$ (b), $x = 0.5$ (c), $x = 0.75$ (d) and $x = 1$ (e). Bar: 100 nm.

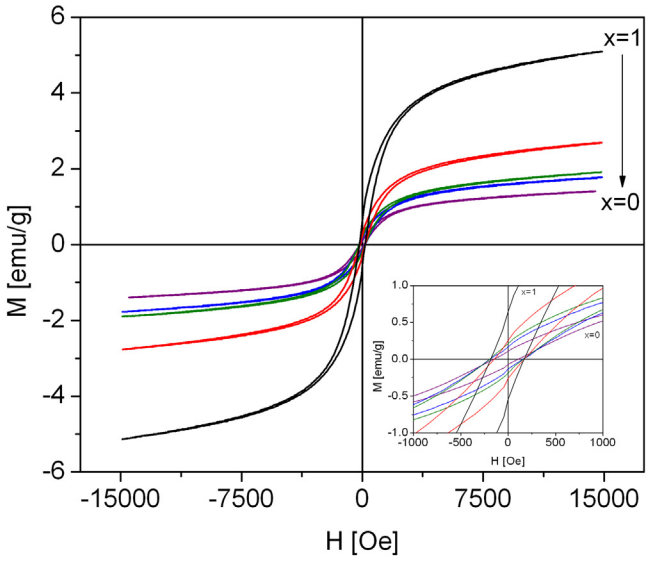

Fig. 5. Hysteresis loops M vs H for the set $Y_xLa_{1-x}FeO_3$. The inset is a close-up of the low-field region. (For interpretation of the references to colour in this figure legend, the reader is referred to the web version of this article.)

the reported values for $YFeO_3$ nanocrystals from Refs. [38,39]. These significant variations in coercivity may be due to dissimilar material microstructures, caused by different synthesis methods for preparing $YFeO_3$ samples. In our case, the presence of SPM particles is probably also contributing to the low observed coercivity. In contrast, for $LaFeO_3$ (YLM-0) the coercivity value agrees with results published earlier (around 100 Oe) [40,41]. In this case, as seen before from Mössbauer spectroscopy results, the presence of SPM particles is lower, so it seems that it does not have effect on the intrinsically low coercivity of $LaFeO_3$.

M_s increases with Y content. This effect has been reported in a previous paper [26] and is understood considering the canting that Y originates when entering and distorting the crystalline structure. Goldschmidt tolerance factor (t) was calculated for all the compositions, using ionic radii from Shannon [42]. The variation of t with x is displayed in Table 2. A maximum value of $t = 1$ is expected for the ideal cubic perovskite structure. A tolerance factor of 0.75 is the limit value for a perovskite-type array [43]. Table 2 shows a decrease of t, due the progressive lattice distortion produced by the substitution of La^{3+} by Y^{3+}. The distortion involves the cooperative tilting of FeO_6 octahedra, enhancing the spin canting and the measured magnetization. In addition, a spin-canting effect associated to particle surface could play a role in this behavior, since the particle agglomeration is more evident for sample YML-1 than for YML-0 (see Fig. 4).

It is known that systems of the type $REFeO_3$ (RE = rare earth) are antiferromagnetically ordered, with a slight canting of Fe spins which originate a weakly ferromagnetic behavior. The Dzyaloshinsky–Moriya antisymmetric exchange is the responsible for the observed canting which renders a net magnetic moment perpendicular to the uniaxial magnetocrystalline anisotropy. Some

Table 2
Coercivity H_c, remanence M_r, saturation magnetization M_s, and tolerance factor t, for the as-milled samples. M_s was calculated by extrapolating M vs $1/H$ to zero.

	H_c (Oe)	M_r (emu/g)	M_s (emu/g)	t
YLM-0	130	0.11	1.65	0.96
YLM-0.25	175	0.17	2.10	0.94
YLM-0.50	175	0.21	2.22	0.91
YLM-0.75	155	0.25	3.15	0.89
YLM-1	175	0.64	5.80	0.86

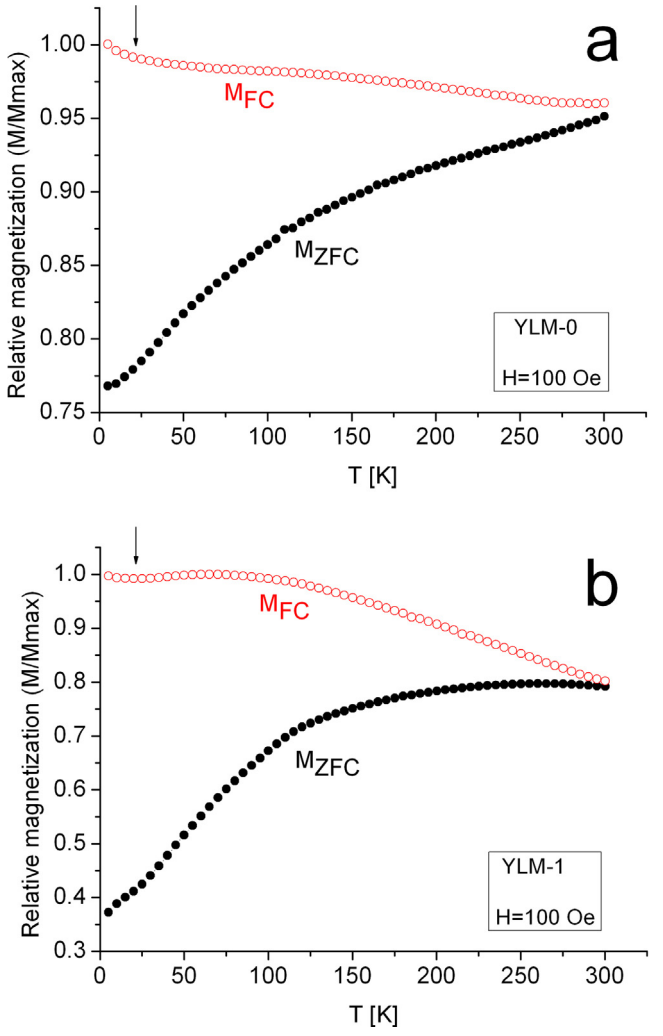

Fig. 6. Zero field cooling/Field cooling curves for samples YLM-0 (a) and YLM-1 (b), measured with an applied field of 100 Oe.

authors [44] find a mixed behavior of hard and soft anisotropy fields in a single-phase sample of $YFeO_3$. However, that is not the case for our sample, since the corresponding hysteresis loop is typical of a single magnetic phase (Fig. 5). Our results for the hysteresis loop measured for $LaFeO_3$ (sample YLM-0) also differ from that of a nanocrystalline sample prepared by the sonochemical method [45] which does not saturate at 1.6 T.

The changes in zero field cooling and field cooling magnetization (M_{ZFC} and M_{FC}) with T in samples YLM-0 ($LaFeO_3$) and YLM-1 ($YFeO_3$) are shown in Fig. 6 (a) and (b), respectively.

For these samples, M_{ZFC} does not exhibit a defined maximum and both M_{ZFC} and M_{FC} remain non-overlapping up to values beyond 300 K, which suggests a broad distribution of particle sizes. Moreover, a small dip in M_{FC} is observed in the low temperature region (see arrows in Fig. 6). Sasaki et al. [46] have attributed this effect to a superspin glass behavior, in which the spins of particles with mild dipolar interaction and randomness in position freeze collectively into a spin glass phase below a critical temperature. However, other authors also link this feature to a paramagnetic signal from small clusters or atoms dispersed between the particles [47]. In our case, this last interpretation is more adequate, due to the wide particle size distribution in our systems, deduced by Mössbauer spectroscopy results and corroborated ahead.

In order to investigate the energy barrier distribution, the derivative $d(M_{ZFC}-M_{FC})/dT$ is usually calculated and plotted

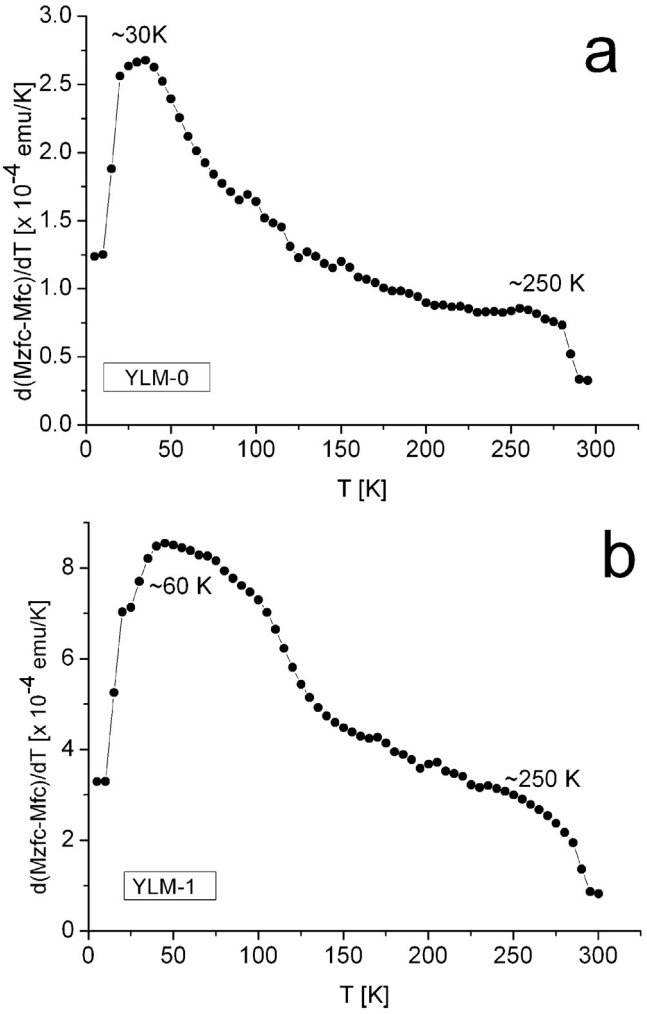

Fig. 7. Blocking temperature distributions calculated for samples YLM-0 (a) and YLM-1 (b).

vs T. When the anisotropy is proportional to the volume (as in this case) the profile of $d(M_{ZFC}–M_{FC})/dT$ vs T (associated with a blocking temperature distribution) is the same as the profile of the size distribution [48]. Fig. 7 shows the calculated distributions for YLM-0 (a) and YLM-1 (b).

Two wide maxima can be noticed in both cases, one at ~250 K and the other at ~30 K and ~60 K for YLM-0 and YLM-1, respectively. A very wide distribution of blocking temperatures can be noticed for both samples.

It is well known that the following relation for conventional magnetometry measuring time ($\tau_m \sim 100$ s) is accepted for slightly-interacting or non-interacting particulate systems,

$$V_{ac} \approx 25\frac{k_B T_B}{K} \quad (1),$$

where V_{ac} is the activation volume, k_B is the Boltzman constant, T_B is the blocking temperature and K is the anisotropy constant. This

Table 3
Anisotropy constants K, blocking temperatures T_B and particles diameters D_{part} calculated from Eq. (1), considering spherical and non-interacting particles.

Sample	Phase	K [erg cm^{-3}]	T_B [K]	D_{part} [nm]
YLM-0	$LaFeO_3$	1.1×10^6	30	1
			250	43
YLM-1	$YFeO_3$	7.6×10^4	50	16
			250	28

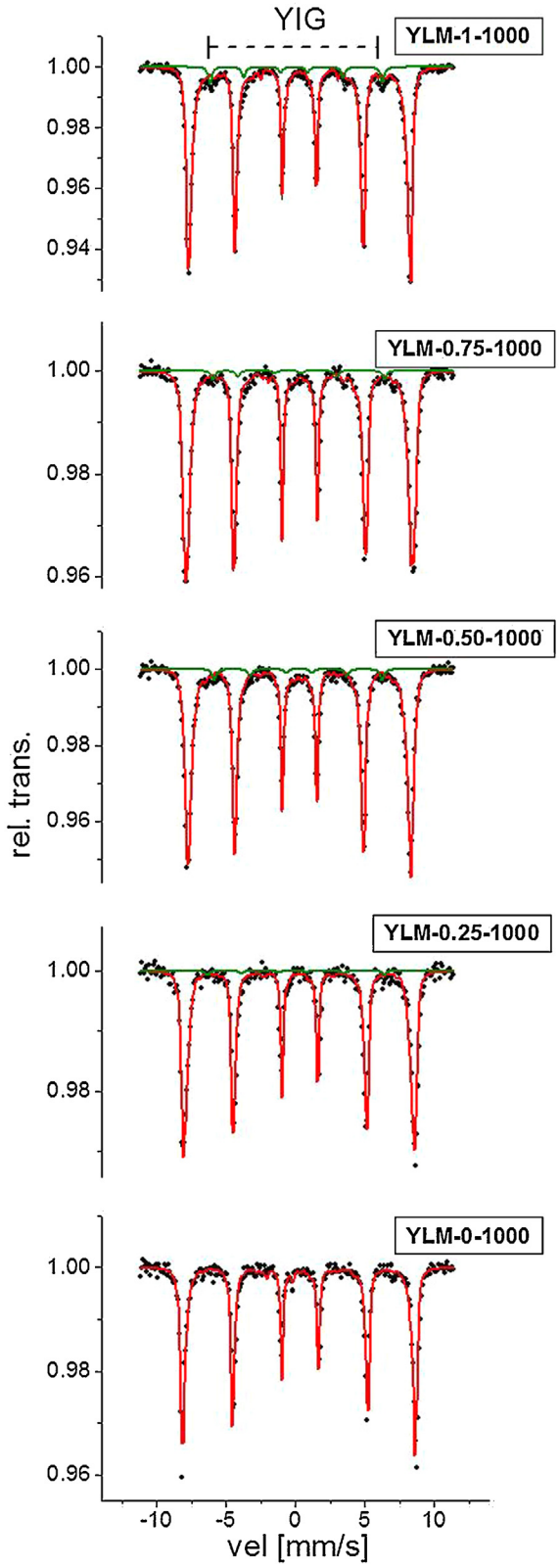

Fig. 8. Mössbauer spectra for the YLM-x-1000 series. (For interpretation of the references to colour in this figure legend, the reader is referred to the web version of this article.)

Table 4
Mössbauer hyperfine parameters for the orthoferrite subspectrum in the YLM-*x*-1000 series.

Sample	Phase	IS (mm/s)	2ε (mm/s)	B_{hf} (T)
YLM-0–1000	$LaFeO_3$	0.37	−0.09	51.93
YLM-0.25–1000	$Y_{0.25}La_{0.75}FeO_3$	0.38	−0.05	51.31
YLM-0.50–1000	$Y_{0.50}La_{0.50}FeO_3$	0.37	−0.02	50.47
YLM-0.75–1000	$Y_{0.75}La_{0.25}FeO_3$	0.36	−0.02	49.55
YLM-1–1000	$YFeO_3$	0.36	−0.01	49.10

equation allows to estimate V_{ac} for the system to overcome the energy barrier at T_B and become superparamagnetic. Even when our systems display an interacting behavior, we can use this result to estimate minimum and maximum activation volumes for the blocking temperatures found at lower and higher T, respectively. In our case, since our system is composed of fine particles, we assume that $V_{ac} \sim V_{part}$.

In order to use relation (1), the anisotropy constants K must be known for both samples. The values of K were evaluated using the work of Treves [49] where he concludes that both in $YFeO_3$ and $LaFeO_3$ single-crystals the predominant mechanism responsible for weak ferromagnetism is the antisymmetric exchange interaction and proposes an antisymmetric exchange model which accounts for the value of K for both phases. Using his results and the theoretical densities of $YFeO_3$ and $LaFeO_3$ (5.7 and 6.6 g cm^{-3}, respectively) we obtain $K(YFeO_3) = 7.6 \times 10^4$ erg cm^{-3} and $K(LaFeO_3) = 1.1 \times 10^6$ erg cm^{-3}. The high value of $K(LaFeO_3)$ as compared to $K(YFeO_3)$ is surprising. The iron lattice in $YFeO_3$ is much more distorted than in $LaFeO_3$ (in fact, tolerance factor of Goldschmidt for $LaFeO_3$ is 0.96 and for $YFeO_3$ is 0.86). However, magnetocrystalline anisotropy is probably caused by the distortion of the oxygen octahedra that surround the iron lattice, so it appears that although the iron lattice in $LaFeO_3$ is less distorted than in $YFeO_3$, the oxygen octahedra are more distorted [49].

Considering spherical particles, the above mentioned values for the anisotropy constants and relation (1), different results for V_{ac} (V_{part}) were obtained when considering the blocking temperatures for YLM-0 and YLM-1. The results are summarized in Table 3.

From these results we can infer that particles larger than 43 nm in YLM-0 and 28 nm in YLM-1 would be the ones responsible for the ferromagnetic behavior observed in these samples at RT.

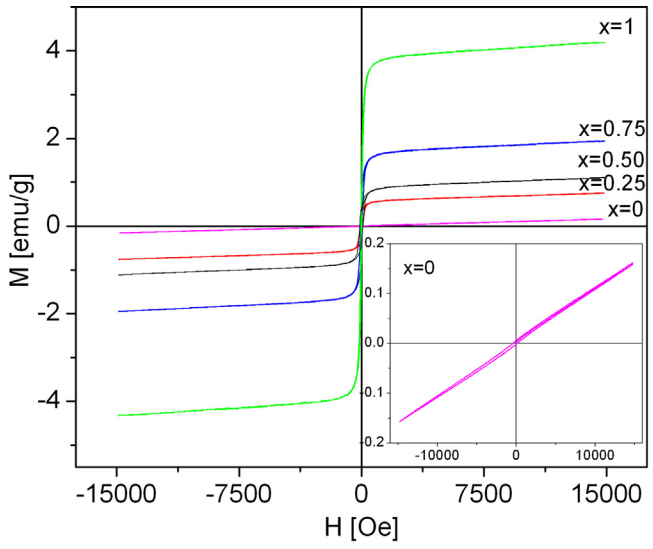

Fig. 9. Hysteresis loops M vs H for the series $Y_xLa_{1-x}FeO_3$ after heating at 1000 °C. The inset is the loop corresponding to $x = 0$. (For interpretation of the references to colour in this figure legend, the reader is referred to the web version of this article.)

The observation of the blocking temperature T_B strongly depends on the time window of the experiment (τ_m). For Mössbauer spectroscopy it is $\tau_m \sim 10^{-8}$ s, much lower than the one for magnetization measurements ($\sim 10^2$ s); that is why T_B values calculated from Mössbauer experiments are larger than those from magnetization analysis. However, Fig. 3 for sample YLM-1 shows that at 20 K the system is not yet totally blocked, confirming there is a wide distribution of blocking temperatures and that the above values, calculated from magnetization results and considering some approximations, are only an estimation to corroborate the wide distribution of particle size. Considering that for Mössbauer Spectroscopy, T_B is the temperature where the SPM contribution and the magnetically split one amount 50% each, it can also be inferred from Table 1 that T_B decreases as the Y content increases in the samples, denoting a smaller critical size of the particles, in agreement with magnetization results.

Fig. 8 shows the Mössbauer spectra for samples YLM calcined at 1000 °C.

Comparison with the as-milled samples reveals the increase of cristallinity and crystallite size produced by the thermal treatment, as also deduced from XRD results (Fig. 1).

As Y content increases, B_{hf} for the orthoferrite subspectrum diminishes (see Table 4). This may be the consequence of a change in the super-transferred hyperfine field because of the loss of some Fe–O–Fe exchange paths.

Another magnetic sextet with a lower value of hyperfine field is observed in the Y-bearing samples. The proportion in which this sextet is present is scarce and it increases with Y content (its relative abundance for sample YLM-1, as calculated from Mössbauer results, is about 11% and lower than 6% for the other samples). This subspectrum is attributed to the secondary phase $Y_3Fe_5O_{12}$; also denominated as yttrium iron garnet (YIG). Mössbauer spectra for this compound at RT display two sextets corresponding to Fe^{3+} at tetrahedral and octahedral sites in the bcc structure, with hyperfine magnetic fields around 49 T and 39 T respectively [50]. In our case, tetrahedral sites are masked by the orthoferrite signal so this phase is more clearly distinguished by the subspectrum assigned to iron in octahedral sites (B_{hf} near 39 T, see Fig. 9). This is also confirmed by XRD, as shown in Fig. 1.

M vs H curves for the series of calcined samples are shown in Fig. 9.

A marked difference can be noticed between sample YLM-0–1000 and the other members of the series. The linear response of M with H is consistent with the antiferromagnetic behavior of $LaFeO_3$. Comparison with the magnetic loop of the sample before heating (YLM-0 in Fig. 5) confirms the healing of structural defects produced by ball-milling. For the other calcined samples, typical ferromagnetic loops are observed, as a consequence of the contribution of ferrimagnetic YIG, whose concentration in the powders increases with x. Coercivity of these materials decreases continuously from 280 Oe for YLM-0–1000 to 26 Oe for YLM-1–1000, due to the relative increment in the samples of the soft magnetic phase (YIG).

4. Conclusions

High-energy ball-milling of Fe_3O_4–La_2O_3–Y_2O_3 mixtures produces a RT solid state reaction, yielding $Y_xLa_{1-x}FeO_3$ with $0 \leq x \leq 1$. The obtained materials are single-phase, crystallized in submicron agglomerates of nanometric particles. Mössbauer spectra reveal the coexistence of a hyperfine field distribution and a superparamagnetic doublet, which come from the wide size particle distribution existing in the synthesized solids. The magnetic hyperfine field reduces as Y content increases, probably due to a decrease in the average supertransferred hyperfine magnetic field. Relative abundance of both contributions is

controlled by the composition of the orthoferrites. Magnetic states are characterized by a wide distribution of blocking temperatures corresponding to the broad range of particle sizes. RT magnetic properties are consistent with a weak ferromagnetic behavior due to the remaining blocking of the largest particles. Calcination at 1000 °C produces an increase of crystallite size together with the formation of impurities of ferromagnetic YIG (11% for the sample richer in Y).

Magnetism is strongly sensitive to the synthesis method; the role of particle size and interactions between clusters and particles within clusters is decisive.

Acknowledgments

The authors wish to thank CONICET, ANPCyT, UNMdP and Secyt-UNC for their financial support.

References

[1] J.B. Goodenough, Electronic and ionic transport properties and other physical aspects of perovskites, Rep. Prog. Phys. 67 (2004) 1915–1993.
[2] Y.S. Didosyan, H. Hauser, G.A. Reider, J. Nicolics, Sensors and actuators on orthoferrites, Proc. IEEE Sens. 2 (2004) 1032–1035.
[3] X. Ding Lü, Microwave-assisted synthesis of perovskite $ReFeO_3$ (Re: La, Sm, Eu, Gd) photocatalyst, Mater. Sci. Eng. B 171 (2010) 31–34.
[4] A.J. Jacobson, Materials for solid oxide fuel cells, Chem. Mater. 22 (2010) 660–674.
[5] M.A. Ahmed, S.I. El-Dek, Extraordinary role of Ca^{2+} ions on the magnetization of $LaFeO_3$ orthoferrite, Mater. Sci. Eng. B 128 (2006) 30–33.
[6] A.K. Azad, S.-G. Eriksson, J.T.S. Irvine, Structural, magnetic and electrochemical characterization of $La_{0.83}A_{0.17}Fe_{0.5}Cr_{0.5}O_{3-\delta}$ (A = Ba, Ca) perovskites, Mater. Res. Bull. 44 (2009) 1451–1457.
[7] C. Zhu, A. Nobuta, I. Nakatsugawa, T. Akiyama, Solution combustion synthesis of $LaMO_3$ (M = Fe, Co Mn) perovskite nanoparticles and the measurement of their electrocatalytic properties for air cathode, Int. J. Hydrogen Energy 38 (2013) 13238–13248.
[8] F. Rivadulla, Magnetotransporte y resonancia de spin electronico en manganitas, Ph.D. thesis, University of Santiago de Compostela, 2000.
[9] C. Li, K.C.K. Soh, P. Wu, Formability of ABO_3 perovskites, J. Alloys Compd. 372 (2004) 40–48.
[10] R.D. Shannon, Acta Crystallogr. A 32 (1976) 751.
[11] D. Treves, J. Appl. Phys. 36 (1965) 1033–1039.
[12] J. Ma, R. Diallo, A. Stevens, F. Llobet, M.B. Abernathy, R.J. McQueeney, Role of magnetic exchange energy on charge ordering in $R_{1/3}Sr_{2/3}FeO_3$ (R = La, Pr, and Nd), Phys. Rev. B 84 (224) (2011) 115.
[13] Y.S. Didosyan, H. Hauser, H. Wolfmayer, J. Nicolics, P. Fulmek, Sens. Actuators A 106 (2003) 168.
[14] H. Hauser, M. Evanzin Magnetic hysteresis calculation of sensors based on orthoferrites, Sens. Actuators A 129 (2006) 231–234.
[15] Y.S. Didosyan, H. Hauser, G.A. Reider, W. Toriser, J. Appl. Phys. 95 (2004) 7339–7341.
[16] P.V. Gosavi, R.B. Biniwale, Pure phase $LaFeO_3$ perovskite with improved surface area synthesized using different routes and its characterization, Mater. Chem. Phys. 119 (2010) 324–329.
[17] W. Zheng, R. Liu, D. Peng, G. Meng, Hydrothermal synthesis of $LaFeO_3$ under carbonate-containing medium, Mater. Lett. 43 (2000) 19–22.
[18] O. Yamaguchi, H. Takemura, M. Yamashita, Formation of yttrium iron oxides derived from alkoxides, J. Electrochem. Soc. 138 (1991) 1492–1494.
[19] W. Zhang, C. Fang, W. Yin, Y. Zeng, One-step synthesis of yttrium orthoferrite nanocrystals via sol–gel auto-combustion and their structural and magnetic characteristics, Mater. Chem. Phys. 137 (2013) 877–883.
[20] D. Du Buolay, E.N. Maslem, V.A. Streltsov, N. Ishizawa, A synchrotron X-ray study of the electron density of $YFeO_3$, Acta Cryst. B 51 (1995) 921–929.
[21] V. Buscaglia, F. Caracciolo, C. Bottino, M. Leoni, P. Nanni, Reaction diffusion in the Y_2O_3–Fe_2O_3 system, Acta Mater. 45 (1999) 1213–1224.
[22] D. Gil, M.C. Navarro, M.C. Lagarrigue, J. Guimpel, R.E. Carbonio, M.I. Gómez, Synthesis and structural characterization of perovskite $YFeO_3$ by thermal decomposition of a cyano complex precursor $Y[Fe(CN)_6]4H_2O$, J. Therm. Anal. Calorim. 103 (2011) 889–896.
[23] S. Mathur, M. Veith, R. Rapalaviciute, H. Shen, G.F. Goya, W.L.M. Filho, T.S. Berquo, Molecule derived synthesis of nanocrystalline $YFeO_3$ and investigations on its weak ferromagnetic behavior, Chem. Mater. 16 (2004) 1906.
[24] L.J. Downie, W. Goff, S.D. Forder, J.E. Parker, F.D. Morrison, P. Lightfoot, Structural, magnetic and electrical properties of the hexagonal ferrites $MFeO_3$ (M = Y, Yb, In), J. Solid State Chem. 190 (2012) 52–60.
[25] A.A. Cristóbal, P.M. Botta, P.G. Bercoff, J.M. Porto López, Mat. Res. Bull. 44 (2009) 1036–1040.
[26] A.A. Cristóbal, P.M. Botta, E.F. Aglietti, M.S. Conconi, P.G. Bercoff, J.M. Porto López, Mat. Chem. Phys. 130 (2011) 1275–1279.
[27] D.L. Zhang, Prog. Mater. Sci. 49 (2004) 537–560.
[28] S.L. James, C.J. Adams, C. Bolm, D. Braga, P. Collier, T. Friščić, Chem. Soc. Rev. 41 (2012) 413–447.
[29] V. Sepelák, A. Düvel, M. Wilkening, K.-D. Becker, P. Heitjans, Mechanochemical reactions and syntheses of oxides, Chem. Soc. Rev. 42 (2013) 7507–7520.
[30] V. Sepelák, D. Baabe, D. Mienert, D. Schultze, F. Krumeich, F.J. Litterst, K.D. Becker, J. Magn. Magn. Mater. 257 (2003) 377.
[31] T.I. Arbuzova, B.A. Gizhevski, R.G. Zakharov, S.A. Petrova, N.M. Chebotaev, Magnetic Susceptibility of Nanostructural Manganite $LaMnO_{3+\delta}$ produced by mechanochemistry method, Phys. Sol. State 50 (2008) 1487–1494.
[32] V. Kusigerski, M. Tadić, V. Spasojević, B. Antić, D. Marković, S. Bošković, B. Matović, High coercivity of γ-Fe_2O_3 nanoparticles obtained by a mechanochemically activated solid-state displacement reaction, Scr. Mater. 56 (2007) 883–886.
[33] G.J. Long, T.E. Cranshaw, G. Longworth, Mössbauer Eff. Ref. Data J. 6 (1983) 42.
[34] R.A. Brand, Normos program, Internat. Rep. Angewandte Physik, University, Duisburg, 1987.
[35] A. Delmastro, D. Mazza, S. Ronchetti, M. Vallino, R. Spinicci, P. Brovetto, M. Salis, Mat. Sci. Eng. B 79 (2001) 140–145.
[36] G.W. Durbin, C.E. Johnson, M.F. Thomas, J. Phys. C: Solid State Phys. 8 (1975) 3051–3057.
[37] R. Maiti, S. Basu, D. Chakravorty, J. Mag. Magn. Mater. 321 (2009) 3274–3277.
[38] J. Wu, J.C. Yu, L.Z. Zhang, X.C. Wang, S.K. Li, Selective self-propagating combustion synthesis of hexagonal and orthorhombic nanocrystalline yttrium iron oxide, J. Solid State Chem. 177 (2004) 3666.
[39] W. Zhang, C. Fang, W. Yin, Y. Zeng, Mat. Chem. Phys. 137 (2013) 877–883.
[40] X. Qi, J. Zhou, Z. Yue, Z. Gui, L. Li, Mat. Chem. Phys. 78 (2002) 25–29.
[41] T. Fujii, I. Matsusue, D. Nakatsuka, M. Nakanishi, J. Takada, Mat. Chem. Phys. 129 (2011) 805–809.
[42] R.D. Shannon, Acta Cryst. A 32 (1976) 751–767.
[43] V.M. Goldschmidt, Naturwissenschaften 14 (1926) 477–485.
[44] E. Lima Jr., T.B. Martins, H.R. Rechenberg, G.F. Goya, C. Cavelius, R. Rapalaviciute, S. Hao, S. Mathur, J. Mag. Magn. Mat. 320 (2008) 622–629.
[45] M. Sivakumar, A. Gedanken, W. Zhong, Y.H. Jiang, Y.W. Du, I. Brukental, D. Bhattacharya, Y. Yeshurun, I. Nowik, J. Mater. Chem. 14 (2004) 764–769.
[46] M. Sasaki, P.E. Jönsson, H. Takayama, H. Mamiya, Phys. Rev. B 71 (2005) 104405.
[47] O. Petracic, X. Chen, S. Bedanta, W. Kleemann, S. Sahoo, S. Cardoso, P. Freitas, J. Mag. Magn. Mat. 300 (2006) 192–197.
[48] M. Knobel, W.C. Nunez, L.M. Socolovsky, E. De Biasi, J.M. Vargas, J.C. Denardin, J. Nanosci. Nanotech. 8 (2008) 2836–2857.
[49] D. Treves, Phys. Rev. 125 (1962) 1843–1852.
[50] M. Ristić, I. Nowik, S. Popović, I. Felner, S. Musić, Mater. Lett. 57 (2003) 2584–2590.